Manuscript prepared for The Cryosphere
with version 2014/09/16 7.15 Copernicus papers of the LaTeX class copernicus.cls.
Date: 1 September 2015

On the influence of the treatment of friction at the grounding line

O. Gagliardini[1,2,3], J. Brondex[1,2], F. Gillet-Chaulet[1,2], L. Tavard[1,2], V. Peyaud[1,2], and G. Durand[1,2]

[1]Univ. Grenoble Alpes, LGGE, 38041 Grenoble, France
[2]CNRS, LGGE, 38041 Grenoble, France
[3]Institut Universitaire de France, Paris, France

Correspondence to: O. Gagliardini (olivier.gagliardini@ujf-grenoble.fr)

Abstract. The dynamical contribution of marine ice sheets to sea level rise is largely controlled by grounding line (GL) dynamics. Seroussi et al. (2014) emphasised the sensitivity of numerical ice flow model results to the practical implementation of the friction of the ice on its bed in the very close vicinity of the GL. Elmer/Ice is a reference finite element (FE) ice flow model used in recent marine ice sheet model intercomparison (MISMIP) exercises. In the model, the GL is defined as the nodes where the ice is in contact with the bedrock but belong to both grounded and floating elements. Inherently to the FE method, computing the contribution of the friction by element requires evaluating the friction at the integration points. In Elmer/Ice, this is done by interpolating the values of the friction parameter C prescribed at the nodes. In this brief communication, we discuss and compare three alternative ways to prescribe the friction at the GL: (i) C is prescribed and non null at the GL nodes, (ii) C is set to zero at the GL nodes, and (iii) C is discontinuous at the GL nodes (i.e. is prescribed and non null for grounded elements and otherwise null). So far, all published results using Elmer/Ice were obtained with the first method. Using the MISMIP3d diagnostic experiment, we first show that the three methods lead to significantly different velocity fields for the mesh resolution adopted in Pattyn et al. (2013). We then show that these methods also lead to different steady state GL positions and different transient behaviours, but that these differences decrease when the mesh refinement is increased. Such model sensitivity to the methods discussed here is certainly specific to the high friction prescribed in the MISMIP experiments and should be smaller in real setups where friction in the vicinity of the GL would be expected to be lower. Results obtained with the three methods, for higher resolutions than previously published, are available as Supplement for future comparisons.

1 Introduction

Marine terminating glaciers in Antarctica and Greenland control the dynamical contribution of these ice sheets to sea level rise. Among the processes at play, the retreat of the grounding line (GL) has a major impact on this dynamical contribution. Accurate modelling of GL dynamics is therefore a precondition for prognostic simulations of the future of ice sheets in a warming climate. Previous works have emphasised the importance of the mesh resolution around the GL (Vieli and Payne, 2005; Durand et al., 2009a, b; Pattyn et al., 2012) and how the friction is interpolated in the vicinity of the GL (Gladstone et al., 2012; Seroussi et al., 2014; Leguy et al., 2014). Two recent intercomparison exercises were designed to compare and test the ability of ice-sheet models to resolve the advance and retreat of the GL based on different perturbations. MISMIP was dedicated to two-dimensional flow line geometry (Pattyn et al., 2012) and used an analytical solution (Schoof, 2007), whereas MISMIP3d was a fully three-dimensional setup (Pattyn et al., 2013).

Elmer/Ice was the only Stokes model to perform the MISMIP experiment 3a (Pattyn et al., 2012) and it was one of only two Stokes models to perform the whole MISMIP3d experiments (Pattyn et al., 2013). Moreover, in the latter intercomparison exercise, the diagnostic experiment P75D was directly build from the geometry obtained with Elmer/Ice after the 100 year perturbation experiment. As the only Stokes model to perform the two intercomparison exercises, Elmer/Ice results are currently used as references for comparison with other models based on lower order Stokes equations (e.g. Feldmann et al., 2014). The results of the MISMIP and MISMIP3d intercomparisons obtained with Elmer/Ice have also been used as benchmarks to test Stokes models during their development.

Using a finite element lower order Stokes model (Shallow Shelf Approximation, SSA), Seroussi et al. (2014) compared various parameterisations of the GL position. Using the SSA, the GL position is directly evaluated from the floatation criterion and can therefore be located at any point of the domain and not only at the element nodes. In this way, the basal friction can be evaluated with a subgrid resolution. Their results revealed the high sensitivity of the GL dynamics to the treatment of basal friction in the close vicinity of the GL and also showed that sub-element parametrisation of the GL significantly reduces the sensitivity of the results to the mesh size at the GL. The proposed methods, by estimating the GL position at a subgrid scale, acts similarly than an increased mesh resolution around the GL, but without the numerical cost associated with remeshing when the GL is moving.

Unfortunately, for the Stokes problem, sub-element parametrisation cannot be applied to solve the contact between the ice and its bed. Indeed, the contact condition can only be evaluated at the element nodes. Therefore, the only way to improve the accuracy of the model is to increase the mesh refinement in the close vicinity of the GL (Durand et al., 2009b). However, even if a sub-element parameterisation of the GL cannot be used, there is more than one possible way of treating the friction in the vicinity of the GL.

The aim of this paper is to present three possible ways to apply friction at the GL and the resulting differences in terms of GL dynamics for the well-defined experiments MIMSIP and MISMIP3d. First we present the three methods and their specificities. Then, using MISMIP and MISMIP3d setups, we compare the three methods in advance and retreat configurations of the GL.

2 Friction in the close vicinity of the GL

Elmer/Ice uses the finite element method and, by construction, all the field variables are defined as nodal values and so is the GL which follows the edges of the elements. The GL dynamics is solved as a contact problem between the ice and the underlying bed. The effectiveness of the contact is tested for each node belonging on the bed by comparing the residual force of the Stokes equations to the force exerted by the sea water pressure (for more details, see Durand et al., 2009a). By definition, the GL is the ensemble of nodes which are the last in contact with the bedrock, i.e. for which the Stokes residual is strickly larger than the water force. Furthermore, the GL marks the transition between ice in contact with the bedrock, and therefore subject to friction, and ice in contact with the ocean with a free slip condition.

Three modelling strategies can be used to impose this transition at the GL between the slip condition to the free-slip condition (see Fig. 1). The first strategy is assuming that the GL defines the last grounded (LG) nodes and that friction is applied up to the nodes belonging to the GL. In the second, the nodes belonging to the GL are assumed to be the first floating (FF) nodes and are already freely slipping. The third strategy assumes that the friction is discontinuous (DI) at the nodes belonging to the GL: friction at these nodes is only applied if integrating over an element where all other nodes are also in contact with the bedrock but a free slip condition is applied if the node belongs to an element where at least one node is in contact with the ocean. The three methods are illustrated in a two-dimensional flow line configuration in Fig. 1.

To build the finite element system to be solved, the friction needs to be interpolated at the integration points of each element. For the LG method, the first elements in contact with the ocean are therefore undergoing some friction due to the interpolation between a non-zero friction value at the nodes belonging to the GL and zero value at the other nodes. On the contrary, for the FF method the friction is lowered in the last elements in contact with the bedrock because of the vanishing friction at the GL nodes. The DI method is therefore certainly the most physical as friction is applied up to the GL but switched off in the first elements in contact with ocean. However the three methods should converge to the same solution when the elements size decreases. Moreover, the three methods should give identical results if the friction at the GL is null, whatever the mesh discretisation. Up to now, all the published Elmer/Ice results were obtained using the LG method (Durand et al., 2009a, b, 2011; Gagliardini et al., 2010, 2013; Favier et al., 2012, 2014; Drouet et al., 2013; Gudmundsson et al., 2012; Pattyn et al., 2012, 2013; Krug et al., 2014). In the following sections, we compare the

three methods using numerical experiments proposed in MISMIP and MISMIP3d, known to present high contrast in friction at the GL. Doing so, the obtained differences between the three methods presented in this paper might be seen as upper bound values for more realistic cases with a smooth transition in friction at the GL.

3 Influence on the flux at the GL

The three methods are first compared using the diagnostic experiment P75D of MISMIP3d. The objective of experiment P75D was to compare the velocity field obtained by the various Stokes approximations for a prescribed glacier geometry. This geometry, the same for all numerical models, was defined as the one obtained with Elmer/Ice at $t = 100$ a for experiment P75S (the last time step of the perturbation experiment, see below and Pattyn et al. (2013) for more details on the experimental setups). We recall that at that time this geometry was obtained using the LG method. Exactly the same mesh as in Pattyn et al. (2013) is used here to compare the three methods on this diagnostic experiment.

In Pattyn et al. (2013), the boundary condition (BC) applied at the base of the ice-shelf for the diagnostic experiment was not specified. If this condition is clear for lower-order Stokes models (i.e. for vertically integrated models), this is not the case when solving for the full-Stokes solution. In the next part, the possible BCs to be applied at the base of the ice-shelf are presented. The velocity field obtained with the three methods for interpolating the friction at the GL are then compared.

3.1 BC below ice-shelf for a diagnostic simulation

In this part we give more details about the different possibilities for the BC at the base of the ice-shelf. Which BC to be applied was not specified for the diagnostic experiment in Pattyn et al. (2013). For a Stokes *prognostic* simulation, assuming no accretion/melting, Durand et al. (2009a) have shown that the following BC should be applied at the base of the ice-shelf (BC1):

$$\sigma_{\mathrm{nn}}|_{\mathrm{b}} = -\rho_{\mathrm{w}} g (l_{\mathrm{w}} - z_{\mathrm{b}}) + C_{\mathrm{n}} u_{\mathrm{n}}, \tag{1}$$

where $\sigma_{\mathrm{nn}}|_{\mathrm{b}}$ is the normal Cauchy stress applied at the base of the ice-shelf, l_{w} and z_{b} are the sea and ice-shelf bottom elevations, respectively, ρ_{w} the water density, g the gravity, $u_{\mathrm{n}} = \boldsymbol{u} \cdot \boldsymbol{n}$ the normal component of the ice velocity and $C_{\mathrm{n}} = \rho_{\mathrm{w}} g \sqrt{1 + (\partial z_{\mathrm{b}}/\partial x)^2 + (\partial z_{\mathrm{b}}/\partial y)^2} \mathrm{d}t$. As explained in Durand et al. (2009a), C_{n} acts like a damper on the bottom interface so that the normal stress induced by $C_{\mathrm{n}} u_{\mathrm{n}}$ will counteract the buoyancy stress and will avoid too large velocity that would arise even for a small buoyancy disequilibrium.

For a Stokes *diagnostic* simulation, one can think about two other BC for the ocean/ice interface. For all of them we implicitly assume that there is no melting or marine ice accretion below the ice-shelf.

The first is deduced from the free surface evolution assuming a steady-state geometry and no melting or accretion. Under such hypotheses, the bottom free surface evolution reduces to the simple Dirichlet BC (BC2):

$$u_{\mathrm{n}} = \boldsymbol{u} \cdot \boldsymbol{n} = 0. \tag{2}$$

The second, a Neumann BC, assumes the buoyancy equilibrium at the interface ice/ocean (BC3):

$$\sigma_{\mathrm{nn}}|_{\mathrm{b}} = -\rho_{\mathrm{w}} g (l_{\mathrm{w}} - z_{\mathrm{b}}). \tag{3}$$

BC1 derives from BC3 with an implicit evaluation of z_{b} at $t + \mathrm{d}t$ using the free surface equation for z_{b}. Note that vertically integrated models does not require any BC at the base of the ice-shelf for a diagnostic simulation as far as the vertical velocity is not computed.

For a steady-state geometry and assuming no melting or accretion below the ice-shelf, all three BC should give the same velocity field as one expects $u_{\mathrm{n}} = 0$ and the buoyancy equilibrium to be fulfilled. Here, for the diagnostic experiment P75D, because the geometry does correspond to a snapshot of a transient evolution, the ice-shelf is not exactly at the buoyancy equilibrium. This is true for the LG method with which the geometry was obtained, and even worse for the two other methods which have completely different geometries after the 100 year perturbation (see discussion below and Fig. 7). We therefore tested the three possibilities for the bottom ice-shelf BC.

Even for the LG method, no convergence of the non-linear iteration was obtained with the Neumann BC3. This indicates that even a small buoyancy disequilibrium renders the Stokes problem ill-posed. Adding the viscous damper C_{n} to the hydrostatic stress (BC1 given by Eq. 1) has a stabilisation effect and allow convergence. No results are therefore presented for BC3. Results for the two other BCs, BC1 and BC2, are presented in the next part.

3.2 Results fron MISMIP3d P75D

Changes along the x direction of the x component of the surface velocity at $y = 0$ (symmetry axis for the flow and centre for the perturbation of the basal friction parameter) and at $y = 50\,\mathrm{km}$ (side of the domain) are presented for all three methods and for the two BCs BC1 and BC2 in Fig. 2. As can be seen in this figure, the LG method leads to the smallest velocity and the FF method to the largest, while the velocity obtained with the DI method is between the two. The way the friction is interpolated at the GL not only influences the velocity downstream from the GL but also over a few ice thicknesses upstream from the GL. At the GL, the relative difference in velocity between LG and FF methods is as high as $23\,\%$ for $y = 0$ and $17\,\%$ for $y = 50\,\mathrm{km}$. The difference is greater at $y = 0$ than at $y = 50\,\mathrm{km}$ despite less friction at the GL at $y = 0$ than at $y = 50\,\mathrm{km}$. As the vertical gradients of horizontal velocity are small at the GL, similar differences would be expected in ice fluxes trough the GL. As depicted in Fig. 3, these differences in velocity are induced by different distributions of the basal shear stress between the three methods. Figure 3 shows high relative differences of the local

tangential stress between the three methods (larger than 50% at some place), but these differences are located in the close vicinity of the GL and they compensate when integrated over all the bedrock. Indeed, all three methods have the same total traction force at the base, as required by the global equilibrium of the ice mass submitted to the gravity force. As expected, the basal shear stress is overestimated downstream the GL for the LG method relative to the DI method (Fig. 3**a**). This excess of stress downstream the GL for the LG method is compensated by a lower shear stress upstream the GL. The opposite pattern is observed for the FF method relative to the DI method (Fig. 3**b**). If the change in basal stress stays local, the induced changes on the velocity are transported and cumulated downstream, explaining the shape of the curves depicted in Fig. 2. Given the mesh resolution adopted to produce these results, the way the friction law is applied in the very close vicinity of the GL is found to have a significant effect on the velocity field.

The Elmer/Ice velocity solution for experiment P75D in Pattyn et al. (2013) is also shown in Fig. 2 (black curve, named LFA in Pattyn et al., 2013). As Elmer/Ice has been used to design the experiment, the geometry and velocity field were directly extracted from the last time step of the transient experiment P75S. Because of the time-integration scheme in Elmer/Ice, the velocity field was in fact computed from the previous time step geometry ($t - 0.5\,\mathrm{a}$), and not computed as the steady-state solution of the geometry provided. This explains the minor difference between the published velocity solution and the newly computed LG solution (brown thick curve in Fig. 2).

The two solutions for the BC below the ice-shelf give slightly different results for all three methods. As shown in Fig. 2, the horizontal flow at the GL for BC2 is found to be slower by approximately $1\,\%$ than the one for BC1, for all three methods and both at $y = 0$ and $y = 50\,\mathrm{km}$. For BC1, despite its theoretical validity only for transient simulation (time step $\mathrm{d}t$ entering Eq. 1), the results presented in Fig. 2 were obtained assuming an arbitrary time step $\mathrm{d}t = 1\,\mathrm{a}$. Anyway, other realistic choices of $\mathrm{d}t$ would not change significantly the results as the term $C_\mathrm{n} u_\mathrm{n}$ in Eq. (1) is found to be at least 10^3 times smaller than the hydrostatic pressure $-\rho_\mathrm{w} g (l_\mathrm{w} - z_\mathrm{b})$. Because the Dirichlet boundary condition BC2 is certainly the easiest to implement and test, the results for both BCs BC1 and BC2 are given as Supplement. For future comparisons, it would be therefore more consistent to use the results in the Supplement of the present publication, either with the buoyancy BC1 or the Dirichlet BC2 applied at the base of the ice-shelf.

For this diagnostic application, the influence of the mesh discretisation has not been inferred. Nevertheless, as expected theoretically, and as will be shown in the following part, the difference between the three methods should decrease by increasing the mesh refinement in the vicinity of the GL.

4 Influence on the GL dynamics

The previous part has indicated a strong sensitivity of the velocity field to the chosen method to interpolate the friction at the GL, and one might therefore expect similar sensitivity on the GL steady state position and GL dynamics. To study this sensitivity, the three methods are compared using both MISMIP and MISMIP3d experiments.

4.1 MISMIP 3a like experiments

This part presents results on the sensitivity to the mesh resolution using a flow line configuration. For that purpose, the GL dynamics is studied using a set up adapted from experiment 3a of the MISMIP intercomparison exercise (Pattyn et al., 2012). Experiment 3a assumes an overdeepened bedrock, a non-linear Weertman friction law and that the GL is evolved by step changes of the ice fluidity parameter. Previous works have shown that steady-state position of GL could differ slightly depending on whether it is obtained from advancing or retreating GL, but that this difference decreased with an increase in mesh resolution (Durand et al., 2009a). We will therefore compare the three methods in cases of both advance and retreat and with various mesh discretizations. Starting from the ice-sheet geometry given by the semi-analytical solution of Schoof (2007) for steps 1 and step 5 of experiment 3a (see Pattyn et al. (2012) for more details), the ice fluidity for step 3 is then applied and the geometry is evolved until a steady state is obtained, one in advance (from step 1 to step 3) and one in retreat (from step 5 to step 3).

Results are presented in Fig. 4 and in Table 1. These results were obtained using the same type of mesh than the one used for producing the Elmer/Ice MISMIP results, with an evolving resolution along the flow direction (see Durand et al. (2009a) for more details). For all configurations, the LG method leads to the most advanced GL, the FF method to the least advanced GL and the DI method to an intermediate GL position. For a given discretisation, differences on the steady GL position from the three methods are of the same order than differences from advance to retreat (comparison of Fig. 4b and c). For a $200\,\mathrm{m}$ discretization, the difference between the LG and FF methods is $18.2\,\mathrm{km}$ in advance and $21\,\mathrm{km}$ in retreat. The DI position is almost exactly half way between the LG and FF positions. With a $25\,\mathrm{m}$ resolution at the GL, these differences are reduced to less than $2\,\mathrm{km}$ in both advance and retreat. For the purpose of comparison, with a given method, the difference between advance and retreat is around $\approx 26\,\mathrm{km}$ at the resolution of $200\,\mathrm{m}$ and is decreased to less than $3\,\mathrm{km}$ at a resolution of $25\,\mathrm{m}$.

Figure 4a also shows the published Elmer/Ice GL position obtained in advance from step 2 to step 3 in Pattyn et al. (2012). This solution was produced using the same discretisation of $200\,\mathrm{m}$ at the GL, but not exactly the same mesh. Despite the same discretisation at the GL, there is a $3\,\mathrm{km}$ difference with the new LG solution. In line with Durand et al. (2009b), these differences illustrate the sensitivity of the GL position not only to the mesh resolution at the GL, but also to the other

mesh characteristics, and more specifically how strongly the mesh resolution is reduced downstream and upstream the GL.

In the previous analysis, we only focussed on the final steady state position of the GL. Using the same experiments, we accessed the transient response by plotting the GL position as well as the rate of change in the volume above floatation (VAF), as a function of time (see Figs. 5 and 6). Because the initial geometries are the same for the three methods (step 1 and step 5 given by Schoof, 2007), but the steady state solutions are different, it appears that the rate of change of the VAF is mainly controlled by the distance from the steady solution. In other words, the longer the distance between the initial geometry and the steady state, the higher the rate of change of the VAF. For the $25\,\mathrm{m}$ resolution, the different steady state geometries being very close, VAF rate of changes are also very similar.

As expected theoretically, the MISMIP flow line study confirms that, despite a high jump in friction at the GL, all three methods converge to an identical solution as the mesh resolution is improved, but can lead to significantly different solutions for a too coarse mesh.

4.2 MISMIP3d P75S and P75R

The three methods are finally compared using the prognostic experiments of MISMIP3d. This experiment is decomposed in three steps. First, assuming no lateral variation in y, a steady state geometry is obtained for each model. In the second step, P75S, a Gaussian sliding perturbation is introduced precisely at the grounding line and centred on the axis of symmetry at $y = 0$ km. This constant perturbation is applied for the next $100\,\mathrm{years}$. Finally, during the last step, P75R, the perturbation is removed and the GL moves back to its initial steady position. Only the first $100\,\mathrm{years}$ of the removal are studied. Note that for the grounding line to get back to its initial steady state position might take much longer than 100 years as the behaviour in advance and retreat is not symmetrical.

The three methods are first compared using a mesh with similar discretisations in both longitudinal and lateral directions as the one used to obtain the LFA results in Pattyn et al. (2013). The element size of the mesh is varied horizontally along the main flow direction, such that the GL stays in the refined zone during the whole experiment. Because the steady state geometries are different for the three methods, the refined zone lies at different places, and even if all meshes present similar features (same number of nodes, same refinement at the GL), they cannot be identical.

As expected from the results presented in the previous part, the steady GL positions obtained with the three methods are significantly different, the LG solution being more advanced by $\approx 7\,\mathrm{km}$ in comparison to the FF one (see Table 2). It should be noticed that this distance is similar to the one obtained between the LG solution and the LFA solution published in Pattyn et al. (2013), using the same discretisation at the GL but not exactly the same mesh. This gives an indication on how the results are sensitive to the mesh, and not only in the vicinity of the GL. In what follows, the transient response is discussed relative to the steady GL position x_{G_0} of each model. It should however be also

noticed that these differences stay much smaller than the differences obtained between the Stokes and SSA solutions ($\approx 525\,\mathrm{km}$ for the Stokes against $\approx 605\,\mathrm{km}$ for the SAA (Pattyn et al., 2013; Seroussi et al., 2014; Feldmann et al., 2014)).

Figure 7 shows the evolution of the GL during the $100\,\mathrm{years}$ of the perturbation (from 0 to $100\,\mathrm{years}$) and during the same time after the perturbation has been removed (from 100 to $0\,\mathrm{years}$), at $y = 0$ and $y = 50\,\mathrm{km}$. As shown in this figure, the transient responses of the three methods relative to their initial position x_{G_0} are similar during the first $5\,\mathrm{years}$, but then differ significantly. Interestingly, if the LG GL is continuously advancing at $y = 0$, this is not anymore the case for the two other methods. The rapid advance of the FF GL position at $y = 0$ occurring during the first years is then followed by a retreat of almost the same magnitude after 100 years, with a difference lower than $2\,\mathrm{km}$ with the initial GL position, when it is almost $19\,\mathrm{km}$ for the LG one (see Table 2). After the perturbation is removed, the GL starts to move back towards its initial steady state position. Nevertheless, after $100\,\mathrm{years}$ (dashed lines from 100 to 0 a in Fig. 7), the GLs are still far from having reached again the steady state position ($\Delta_{x_G} = 0$). The LG method is the fastest in coming back to its steady state position whereas the FF is the slowest.

Such large differences for the transient response of the three methods can only be explained by a too coarse mesh. The steady solution being reasonably close, and independent of the lateral discretisation of the mesh (no transverse variation of any field so that the steady GL is a straight line perpendicular to the x direction), the source of discrepancy for the transient response certainly arises from the lateral discretisation. The number of lateral elements N_y is only 20 for the previous simulations. The sensitivity of the transient response to the lateral discretisation is investigated by running the same experiment with two finer lateral mesh resolution, everything else being the same. Results for $N_y = 40$ and $N_y = 80$ are presented in Figs. 8 and 9, respectively. As can be seen by comparing Figs. 7–9 (see also Table 2 and Fig. 10), differences in the transient response of the three methods are significantly decreased when the lateral mesh refinement is increased. Nevertheless, even with the finest mesh ($N_y = 80$), the difference between the methods stays relatively important ($\approx 5\,\mathrm{km}$ between LG and FF at the end of the perturbation experiment, but to be compared to $17\,\mathrm{km}$ for $N_y = 20$). Figure 10 indicates that the difference for the three methods between the higher resolution ($N_y = 80$) and the two other mesh refinements ($N_y = 40$ and $N_y = 20$) is smaller for the DI method than the two others. In other words, the DI method seems to be less sensitive to the mesh refinement than the two other methods, certainly because it gives an intermediate solution whatever the mesh resolution. This is one more reason that justify that the DI method should be preferentially adopted for future works. Note however that the decrease in mesh sensitivity is not as high as for the subgrid methods proposed for the SSA (Seroussi et al., 2014).

Higher lateral discretisation were not further explored for computing resource purpose, but this study clearly indicates that, as expected theoretically and shown in the previous part using the flow line setup MISMIP, the difference between the three methods is decreased as the mesh resolution is

increased. Published LFA results (Pattyn et al., 2013) were obtained with a lateral discretisation of $N_y = 20$ elements, which was certainly insufficient as shown by these new results using 40 and 80 lateral elements. For further comparisons, we recommend to use the more accurate results presented in Fig. 9 and provided as Supplement.

5 Conclusions

In this paper, we have presented three methods for the treatment of the friction at the GL for a finite element formulation of the Stokes equations. So far, in all the applications using Elmer/Ice, it was assumed that the friction is applied up to the GL using the LG method. In so doing, the first elements immediately downstream from the GL undergo a little friction even if being in contact with the ocean.

We have shown that the treatment of the friction at the GL has a strong influence on both the velocity field and on the resulting GL dynamics for the mesh resolutions that were used to produce the MISMIP and MISMIP3d results. As expected theoretically, differences between the three methods are shown to decrease as the mesh resolution is increased, but these differences remains substantial when using mesh resolutions numerically affordable for usual 3D applications. Even for the smallest refinements accessed for the three-dimensional test case, differences are still observed. However, these differences are much smaller than those between Stokes and lower-order models. This give an indication on the model error to be expected when performing GL dynamics simulations with a Stokes model. Moreover, using MISMIP3d experiment, the lateral refinement is shown to have also a significant influence on the transient behaviour. All these results were obtained using the MISMIP and MISMIP3d setups, which are known to present a very high friction at the GL.

Because the GL is in contact with the ocean, one would expect basal friction to vanish at the GL, i.e. that the friction parameter C tends to zero as the upstream distance to the GL tends to zero. In such a case, if $C = 0$ at the GL, it is clear that all three methods (LG, DI and FF) would be identical and therefore result in the same solution whatever the mesh resolution. Consequently, we expect that for more realistic applications, the sensitivity of the model results to the choice of the friction treatment at the GL would be smaller. The methods proposed by Pattyn et al. (2006), Leguy et al. (2014), Tsai et al. (2015) and Gladstone et al. (2015) present interesting approaches in that direction. Future intercomparison exercices should adopt such approaches to avoid too large jump in friction at the GL and allow the comparison of the different models on more realistic setups. In any case, we recommend to use the discontinuous DI method which is certainly the most realistic and the less sensitive to the mesh refinement of the three. We also recommend to use these newly published results with finer mesh resolutions for future model comparison.

The Supplement related to this article is available online at

doi:10.5194/tc-0-1-2015-supplement.

Acknowledgements. This study was funded by the Agence Nationale pour la Recherche (ANR) through the SUMER, Blanc SIMI 6-2012. The new simulations presented in this paper have been done using the high-performance computing resources of CINES (Centre Informatique National de l'Enseignement Supérieur, France) under allocations 2015-016066 made by GENCI (Grand Equipement National de Calcul Intensif).

References

Drouet, A.-S., Docquier, D., Durand, G., Hindmarsh, R., Pattyn, F., Gagliardini, O., and Zwinger, T.: Grounding line transient response in marine ice sheet models, The Cryosphere, 7, 395–406, 2013.

Durand, G., Gagliardini, O., de Fleurian, B., Zwinger, T., and Le Meur, E.: Marine ice sheet dynamics: Hysteresis and neutral equilibrium, J. Geophys. Res. (Earth Surface), 114, F03 009, doi:doi:10.1029/2008JF001170, 2009a.

Durand, G., Gagliardini, O., Zwinger, T., Le Meur, E., and Hindmarsh, R. C. A.: Full-Stokes modeling of marine ice-sheets: influence of the grid size, Annals of Glaciology, 52, 109–114, doi:doi:10.3189/172756409789624283, 2009b.

Durand, G., Gagliardini, O., Favier, L., Zwinger, T., and Le Meur, E.: Impact of bedrock description on modeling ice sheet dynamics, Geophysical Research Letters, 38, L20 501, doi:doi:10.1029/2011GL048892, 2011.

Favier, L., Gagliardini, O., Durand, G., and Zwinger, T.: A three-dimensional full Stokes model of the grounding line dynamics: effect of a pinning point beneath the ice shelf, The Cryosphere, 6, 101–112, doi:doi:10.5194/tc-6-101-2012, 2012.

Favier, L., Durand, G., Cornford, S., Gudmundsson, G., Gagliardini, O., Gillet-Chaulet, F., Zwinger, T., Payne, A., and Le Brocq, A.: Retreat of Pine Island Glacier controlled by marine ice-sheet instability, Nature Climate Change, 4, 117–121, doi:doi:10.1038/nclimate2094, 2014.

Feldmann, J., Albrecht, T., Khroulev, C., Pattyn, F., and Levermann, A.: Resolution-dependent performance of grounding line motion in a shallow model compared with a full-Stokes model according to the MISMIP3d intercomparison, Journal of Glaciology, 60, 353–360, 2014.

Gagliardini, O., Durand, G., Zwinger, T., Hindmarsh, R., and Le Meur, E.: Coupling of ice-shelf melting and buttressing is a key process in ice-sheets dynamics, Geophysical Research Letters, 37, L14 501, doi:doi:10.1029/2010GL043334, 2010.

Gagliardini, O., Zwinger, T., Gillet-Chaulet, F., Durand, G., Favier, L., de Fleurian, B., Greve, R., Malinen, M., Martín, C., Råback, P., Ruokolainen, J., Sacchettini, M., Schäfer, M., Seddik, H., and Thies, J.: Capabilities and performance of Elmer/Ice, a new-generation ice sheet model, Geoscientific Model Development, 6, 1299–1318, doi:10.5194/gmd-6-1299-2013, http://www.geosci-model-dev.net/6/1299/2013/, 2013.

Gladstone, R. M., Lee, V., Rougier, J., Payne, A. J., Hellmer, H., Le Brocq, A., Shepherd, A., Edwards, T. L., Gregory, J., and Cornford, S. L.: Calibrated prediction of Pine Island Glacier retreat during the 21st and 22nd centuries with a coupled flowline model, Earth and Planetary Science Letters, 333, 191–199, 2012.

Gladstone, R. M., Warner, R., Budd, W., Galton-Fenzi, B., Gagliardini, O., Zwinger, T., and Greve, R.: Marine ice sheet model performance depends on basal sliding physics and sub-shelf melting, The Cryosphere, in preparation, 2015.

Gudmundsson, G. H., Krug, J., Durand, G., Favier, L., and Gagliardini, O.: The stability of grounding lines on retrograde slopes, The Cryosphere, 6, 1497–1505, doi:10.5194/tc-6-1497-2012, http://www.the-cryosphere.net/6/1497/2012/, 2012.

Krug, J., Weiss, J., Gagliardini, O., and Durand, G.: Combining damage and fracture mechanics to model calving, The Cryosphere, 8, 2101–2117, 2014.

Leguy, G., Asay-Davis, X., and Lipscomb, W.: Parameterization of basal hydrology near grounding lines in a one-dimensional ice sheet model, The Cryosphere, 8, 1239–1259, 2014.

Table 1. Experiment MISMIP 3a: steady GL position for step 3 in meter for the three methods in advance and in retreat. Obtained positions which are not a multiple of the mesh discretisation is the result of the adaptive mesh technics.

Method	25 m	50 m	100 m	200 m
LG advance	714 579	713 900	711 400	713 200
LG retreat	716 158	719 058	726 433	741 600
DI advance	713 550	710 483	706 400	705 000
DI retreat	715 860	717 068	720 200	728 100
FF advance	712 550	706 800	705 500	695 000
FF retreat	715 194	712 817	717 633	720 600

Pattyn, F., Huyghe, A., De Brabander, S., and De Smedt, B.: Role of transition zones in marine ice sheet dynamics, J. Geophys. Res, 111, F02 004, doi:doi:10.1029/2005JF000394, 2006.

Pattyn, F., Schoof, C., Perichon, L., Hindmarsh, R. C. A., Bueler, E., de Fleurian, B., Durand, G., Gagliardini, O., Gladstone, R., Goldberg, D., Gudmundsson, G. H., Lee, V., Nick, F. M., Payne, A. J., Pollard, D., Rybak, O., Saito, F., and Vieli, A.: Results of the Marine Ice Sheet Model Intercomparison Project, MISMIP, The Cryosphere, 6, 573–588, doi:10.5194/tc-6-573-2012, 2012.

Pattyn, F., Perichon, L., Durand, G., L., F., Gagliardini, O., Hindmarsh, R. C. A., Zwinger, T., Albrecht, T., Cornford, S., Docquier, D., Fürst, J. J., Golberg, D., Gudmundsson, G. H., Humbert, A., Hütten, M., Huybrechts, P., Jouvet, G., Kleiner, T., Larour, E., Martin, D., Morlighem, M., Payne, A. J., Pollard, D., Rückamp, M., Rybak, O., Seroussi, H., Thoma, M., and Wilkens, N.: Grounding-line migration in plan-view marine ice-sheet models: results of the ice2sea MISMIP3d intercomparison, J. Glaciol., 59, 410–422, doi:10.3189/2013JoG12J129, 2013.

Schoof, C.: Ice sheet grounding line dynamics : Steady states, stability, and hysteresis, Journal of Geophysical Research, 112, doi:10.1029/2006JF000664, 2007.

Seroussi, H., Morlighem, M., Larour, E., Rignot, E., and Khazendar, A.: Hydrostatic grounding line parameterization in ice sheet models, The Cryosphere, 8, 2075–2087, doi:10.5194/tc-8-2075-2014, http://www.the-cryosphere.net/8/2075/2014/, 2014.

Tsai, V. C., Stewart, A. L., and Thompson, A. F.: Marine ice-sheet profiles and stability under Coulomb basal conditions, Journal of Glaciology, 61, 205–215, 2015.

Vieli, A. and Payne, A.: Assessing the ability of numerical ice sheet models to simulate grounding line migration, J. Geophys. Res, 110, doi:10.1029/2004JF000202, 2005.

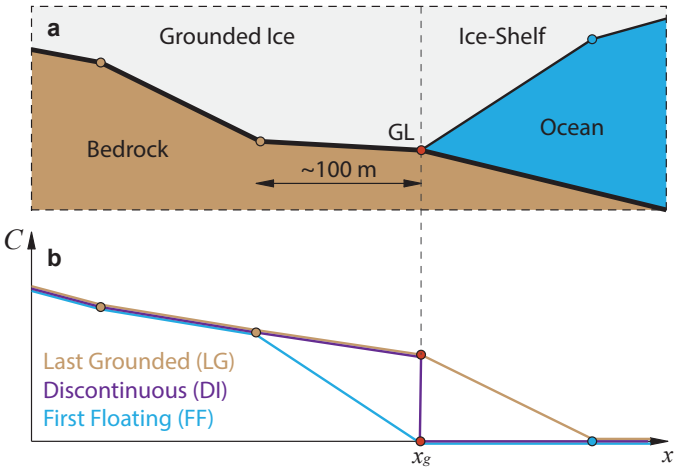

Figure 1. Two-dimensional schematic explanation of the three different alternatives to impose the friction in the close vicinity of the GL. **(a)** Zoom on the triple junction point between ice, bedrock and ocean, defined as the GL (red dot and x_g) and **(b)** changes in the friction parameter C close to the GL, with the three methods: friction is applied at the GL which is then the last grounded node (LG, brown), pure sliding is applied at the GL which is then the first floating node (FF, blue) and the friction is discontinuous at the GL (DI, purple). The coloured dots are the bottom boundary nodes of the finite element mesh: brown in contact with the bedrock, blue in contact with the ocean and red at the GL.

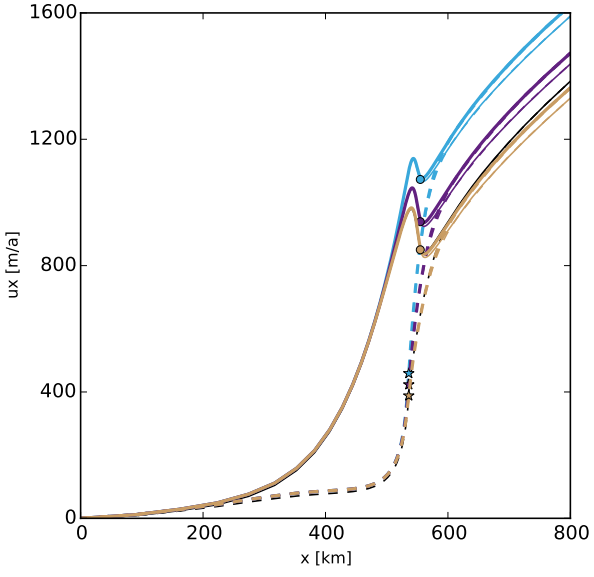

Figure 2. Experiment MISMIP3d P75D: surface velocity along the x direction for the three different methods: LG (brown), DI (purple) and FF (blue) on the symmetry axis ($y = 0$; continuous line) and on the free-slip boundary ($y = 50\,\mathrm{km}$, dashed line), for BC (Eq. 1) (thick line) and BC (Eq. 2) (thin line). The LFA Elmer/Ice solution published in Pattyn et al. (2013) is represented in black (mostly hidden by the LG brown thick curve), The signs indicate the GL position in $y = 0$ (dot) and $y = 50\,\mathrm{km}$ (star).

Table 2. Experiment MISMIP3d: initial steady GL position (x_{G_0}, km) and differences between the final ($t = 100$ a) and initial GL positions (Δx_G, km) in $y = 0$ and $y = 50\,\mathrm{km}$, as a function of the method and the number of element along the y direction (N_y). LFA is the Elmer/Ice solution published in Pattyn et al. (2013).

	Last Grounded LG			Discontinuous DI			First Floatinf FF			LFA
N_y	20	40	80	20	40	80	20	40	80	20
x_{G_0}		529.550			526.800			522.350		537.078
$\Delta x_G\|_0$	18.950	16.350	15.050	9.250	10.825	11.950	1.950	6.425	9.900	17.622
$\Delta x_G\|_{50}$	-0.100	-2.750	-3.850	-8.000	-7.050	-6.250	-13.050	-10.250	-7.850	-1.178

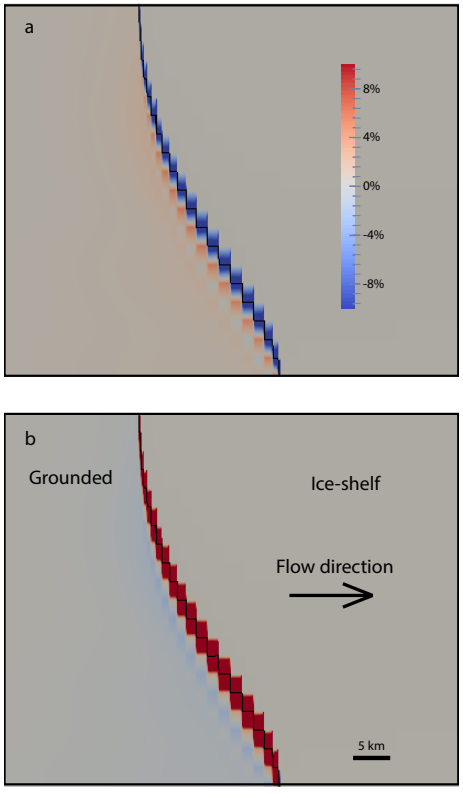

Figure 3. Experiment MISMIP3d P75D: relative difference between the shear stress at the bed for **(a)** the DI and LG methods and **(b)** the DI and FF methods [%]. The black line indicates the GL position. The tangent used to compute the shear stress is the one perpendicular to the transverse direction of the flow.

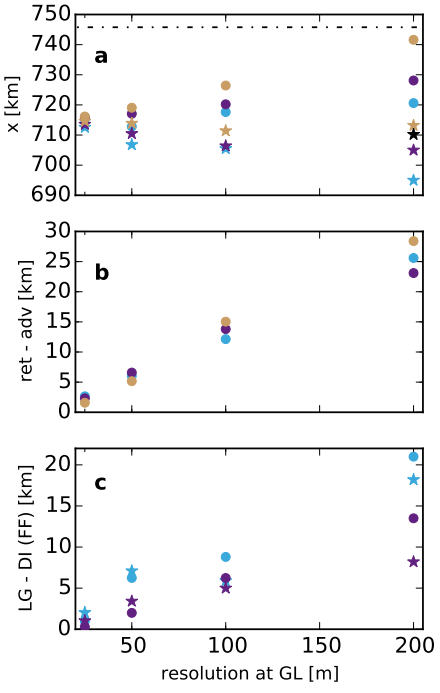

Figure 4. Experiment MISMIP 3a step 3: **(a)** grounding line positions in advance (stars) and retreat (dots) obtained with the three different methods LG (brown), DI (purple) and FF (blue), **(b)** difference in the position of GL in advance and retreat obtained with the three different methods (same colour legend), and **(c)** difference between the LG solutions and the two others, as a function of mesh resolution at the GL. In **(a)**, the black star corresponds to the published GL position for step 3 of experience 3a in Pattyn et al. (2012) and the dot-dashed line is the Schoof (2007) solution.

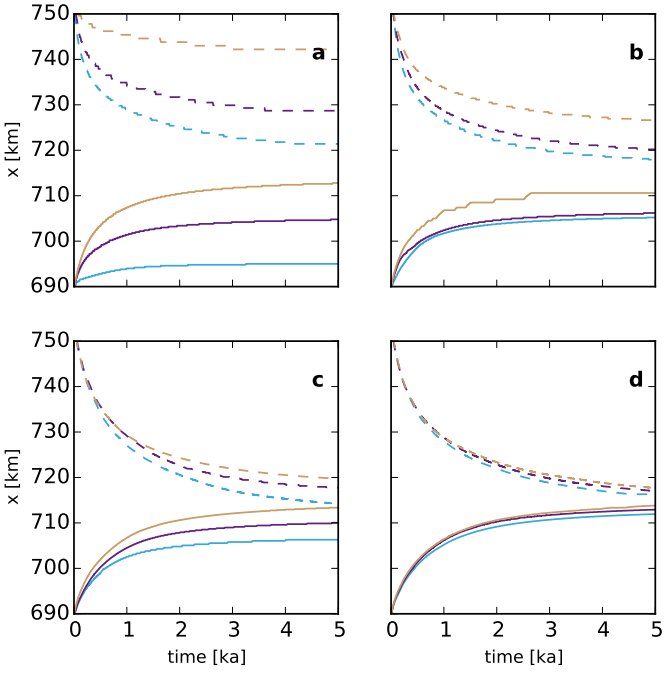

Figure 5. Experiment MISMIP 3a, steps 1 to 3 (advance) and 5 to 3 (retreat): evolution with time of the GL position for the three methods LG (brown), DI (purple) and FF (blue) in advance (solid line) and in retreat (dashed line) for the four resolutions **(a)** $200\,\mathrm{m}$, **(b)** $100\,\mathrm{m}$, **(c)** $50\,\mathrm{m}$ and **(d)** $25\,\mathrm{m}$. The steady state GL positions plotted in Fig. 4 and given in Table 1 are obtained at $t = 10\,\mathrm{ka}$. This figure focusses on the first $5\,\mathrm{ka}$.

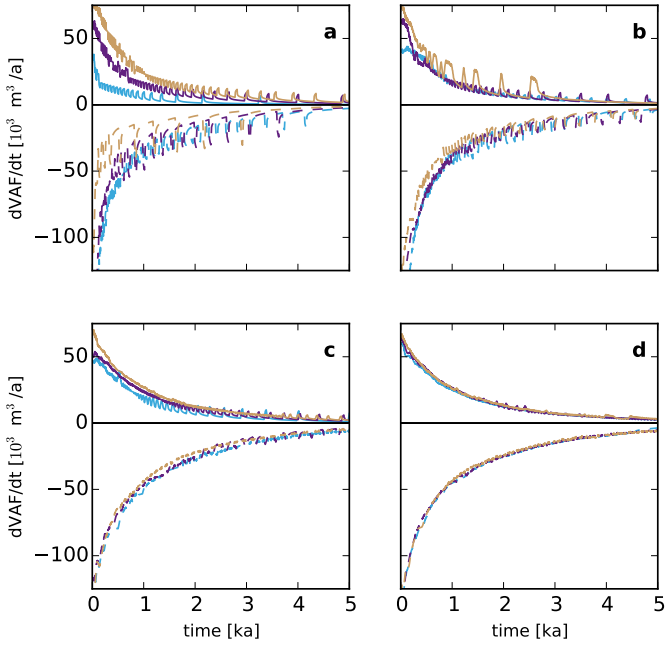

Figure 6. Experiment MISMIP 3a, steps 1 to 3 (advance) and 5 to 3 (retreat): evolution with time of the rate of change of the VAF for the three methods LG (brown), DI (purple) and FF (blue) in advance (solid line) and in retreat (dashed line) for the four resolutions **(a)** $200\,\mathrm{m}$, **(b)** $100\,\mathrm{m}$, **(c)** $50\,\mathrm{m}$ and **(d)** $25\,\mathrm{m}$. The rate of change of the VAF is averaged over a 20 year time window. The steady state GL positions plotted in Fig. 4 and given in Table 1 are obtained at $t = 10\,\mathrm{ka}$. This figure focusses on the first $5\,\mathrm{ka}$.

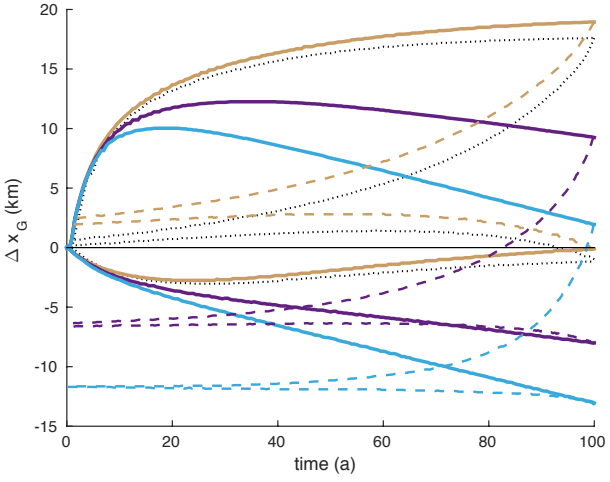

Figure 7. Experiment MISMIP3d P75S and P75R: time-dependent plot of the GL position relative to the steady position x_{G_0} (see Table 2) during (P75S; continuous) and after (P75R; dashed) the basal sliding perturbation, on the symmetry axis ($y = 0$; top curves) and on the free-slip boundary ($y = 50\,\mathrm{km}$; bottom curves) for the three different methods: LG (brown), DI (purple) and FF (blue). The black dotted curve is the GL evolution for the LFA solution published in Pattyn et al. (2013) (LG method and $N_y = 20$). The mesh resolution in the y direction is $N_y = 20$ elements for all simulations.

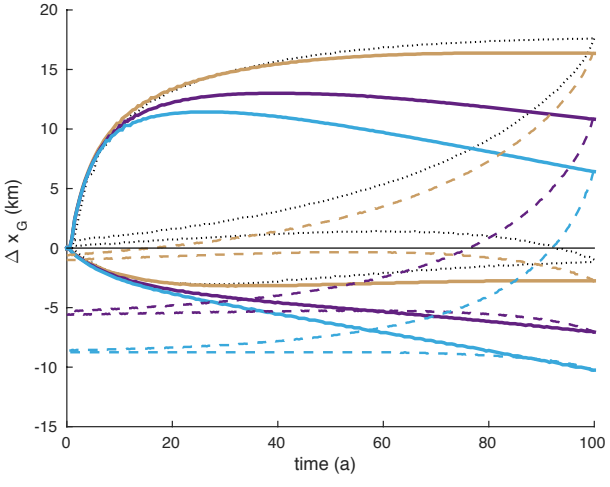

Figure 8. Same as Fig. 7 but for a lateral discretisation of $N_y = 40$ elements.

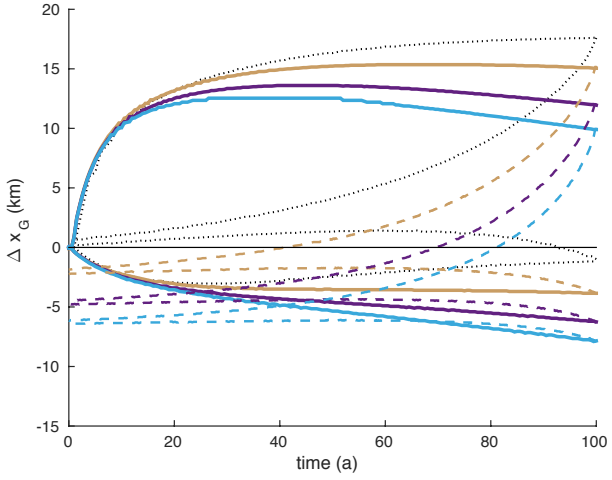

Figure 9. Same as Fig. 7 but for a lateral discretisation of $N_y = 80$ elements.

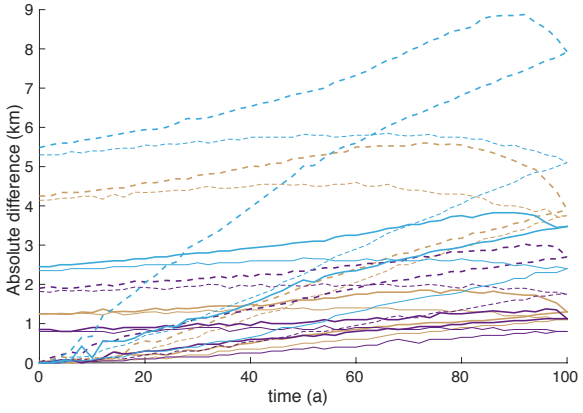

Figure 10. Experiment MISMIP3d P75S and P75R: evolution of the absolute differences in km between the highest resolution ($N_y = 80$) and the two others ($N_y = 40$ continuous line and $N_y = 20$ dashed line) for the three different methods: LG (brown), DI (purple) and FF (blue), on the symmetry axis ($y = 0$; thick curves) and on the free-slip boundary ($y = 50\,\mathrm{km}$; thin curves).